Bioorganic Chemistry 87 (2019) 876–887

Contents lists available at ScienceDirect

Bioorganic Chemistry

journal homepage: www.elsevier.com/locate/bioorg

Fluorescent labeling of ursolic acid with FITC for investigation of its cytotoxic activity using confocal microscopy

Tatiana S. Frolova[a,b,c,d,*], Alla V. Lipeeva[b], Dmitry S. Baev[b,c], Sergey I. Baiborodin[a], Konstantin E. Orishchenko[a], Alexey V. Kochetov[a,c], Olga I. Sinitsyna[a,c]

[a] Federal Research Center Institute of Cytology and Genetics of Siberian Branch of the Russian Academy of Sciences, 10, Lavrentyev Ave., 630090 Novosibirsk, Russia
[b] Novosibirsk Institute of Organic Chemistry of Siberian Branch of the Russian Academy of Sciences, 10, Lavrentyev Ave., 630090 Novosibirsk, Russia
[c] Novosibirsk State University, 2, Pirogov Street, 630090 Novosibirsk, Russia
[d] Federal Research Center of Fundamental and Translational Medicine of Siberian Branch of the Russian Academy of Sciences, 2, Timakov Street, 630117 Novosibirsk, Russia

ARTICLE INFO

Keywords:
Triterpene acids
Ursolic acid
Fluorescence
Cytotoxicity
Akt1/protein kinase B
MDM2/E3 ubiquitin-protein ligase

ABSTRACT

Fluorescent labeling is a widely-used approach in the study of intracellular processes. This method is becoming increasingly popular for studying small bioactive molecules of natural origin; it allows us to estimate the vital intracellular changes which occur under their influence. We propose a new approach for visualization of the intracellular distribution of triterpene acids, based on fluorescent labeling by fluoresceine isothiocyanate. As a model compound we took the most widely-used and best-studied acid in the ursane series – ursolic acid, as this enabled us to compare the results obtained during our research with the available data, in order to evaluate the validity of the proposed method. Experimental tracing of the dynamics of penetration and distribution of the labeled ursolic acid has shown that when the acid enters the cell, it initially localizes on the inner membranes where the predicted target Akt1/protein kinase B – a protein that inhibits apoptosis – is located.

1. Introduction

Triterpenoids comprise a large class of natural compounds, widespread among plants [1]. One of the best studied triterpenoid compounds is 3β-hydroxy-urs-12(13)-en-28-oic (ursolic) acid (Fig. 1), which can be found in significant amounts in plant material [2].

Particular attention has been drawn to ursolic acid's property of having selective cytotoxicity in respect of cancer cells [3]. The acid is capable of inducing apoptosis via a mitochondrial pathway; by activating caspase-3 in M4Beu melanoma cells; by inhibiting the proliferation of cells of the B16 line by arresting the cell cycle [4,5]. It has been noted that a concentration of ursolic acid that is non-toxic for normal cells can induce apoptosis in B16F-10 melanoma cells by inhibiting the transcription factor NF-κB – a universal transcription factor that is involved in the control of gene expression during immune responses, apoptosis and the cell cycle [6,7]. Ursolic acid also shows significant anti-angiogenic activity in models *in vivo* and *in vitro* [8–10]. Studies of the activity of various ursolic acid derivatives show that the modifications at C-3 and C-28 positions enhance the cytotoxic properties, especially introduction of an amino group [11–13]

Study of the mechanisms of anti-cancer action involves the use of a large number of molecular-biological methods. In healthcare, pharmacology and cellular biology, fluorescence methods are frequently used, as they generally represent the fastest and safest approaches [14,15].

Fluorophore attachment is applicable not only for proteins, but also for small bioactive molecules. Thus, the labeled 7-nitro-1,2,3-benzadiazole (NBD) ligand for the opiate receptor σ_2 has been used in the study of the mechanism of its operation in the pancreatic gland oncotransformed BxPC3 line of cells [16]. It has been established that large amounts of this receptor are also present in some other lines of cancer cells where they participate in triggering the apoptosis [17–19], therefore, this is a potential target for therapy of oncological diseases. Adding NBD and Cy5.5 fluorophores to fructose is an approach that has been developed to enable the detection of cancer cells of the lacteal gland. Such cells differ from normal ones in their high levels of the Glut5 transporter and, therefore, an increased fructose uptake [20]. The

Abbreviations: DMSO, dimethyl sulfoxide; FITC, fluoresceine isothiocyanate; UA, ursolic acid; UA*, beta-epimer of fluorescent ladeled ursolic acid; MD, molecular dynamics

* Corresponding author at: Federal Research Center Institute of Cytology and Genetics of Siberian Branch of the Russian Academy of Sciences, 10, Lavrentyev Ave., 630090 Novosibirsk, Russia.
E-mail address: frolova@bionet.nsc.ru (T.S. Frolova).

https://doi.org/10.1016/j.bioorg.2018.11.052
Received 13 August 2018; Received in revised form 26 November 2018; Accepted 29 November 2018
Available online 04 December 2018
0045-2068/

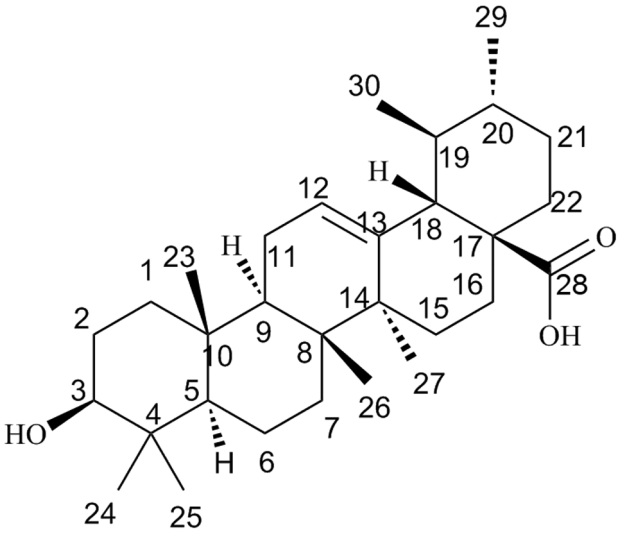

Fig. 1. Ursolic acid.

mechanisms of action of some other anti-proliferative compounds – wortmannin [21] and azathilone [22] – have also been investigated with the help of NBD. The mechanism of the antimalarial effect of 1,2,3-trioxolanes has been examined with the use of the fluorescent dye dansyl chloride [23]. Fluorescence is often used when investigating the intracellular effects of anticancer compounds that cause changes in the cytoskeleton: rhodamine and fluorescein-marked taxoids have turned out to be very convenient for examining the processes of microtubule assembly [24,25]; while phalloidin is used to visualize the reconstruction of actin filaments [26].

In biological research fluorescein isothiocyanate (FITC) has often been used for visualizing the attachment of NH_2- or SH-groups [27–29], because it is non-toxic and allows us to observe such intracellular processes *in vivo*. In this paper we propose a new approach for visualization of the intracellular distribution of triterpene acids, based on fluorescent labeling. As a model compound we took the most widely-used and best-studied acid in the ursane series – ursolic acid, as this enabled us to compare the results obtained during our research with the available data, in order to evaluate the validity of the proposed method.

Table 1
Vina scoring function results: molecular docking of ursolic acid and its fluorescent labeled epimers into Akt1 and MDM2.

Ligand	Binding energy, kcal/mol	
	Akt1	MDM2
Referent*	−8.8	−8.3
Ursolic acid	−8.7	−8.1
α-Epimer	−10.4	−7.4
β- Epimer	−9.7	−8.9

* For each macromolecule we used each own referent ligand: XM1 for Akt1, Nutlin 3a for MDM2.

To synthesize the necessary derivatives, we used a well-known method for the preparation of 3α- and 3β-amino-urs-12(13)-en-28-oic acid **2**, **3** from 3β-hydroxy-urs-12(13)-en-28-oic acid **1** [30] followed by further reaction of the derivatives with fluorescein isothiocyanate **4** (Fig. 2).

Thus, the reaction of 3β-hydroxy-urs-12(13)-en-28-oic acid with the Jones reagent [31] leads smoothly to the formation of 3-oxo-urs-12(13)-en-28-oic acid, which further reacts with ammonium acetate in the presence of sodium cyanoborohydride to form a mixture of the necessary epimers of 3-amino-urs-12(13)-en-28-oic acid **2** and **3** with yields of 20 and 40% respectively for the α and β-forms (after column chromatography and re-crystallization according to the operating procedure [30]).

The key stage in the synthesis of fluorescence labeled 3β-hydroxy-

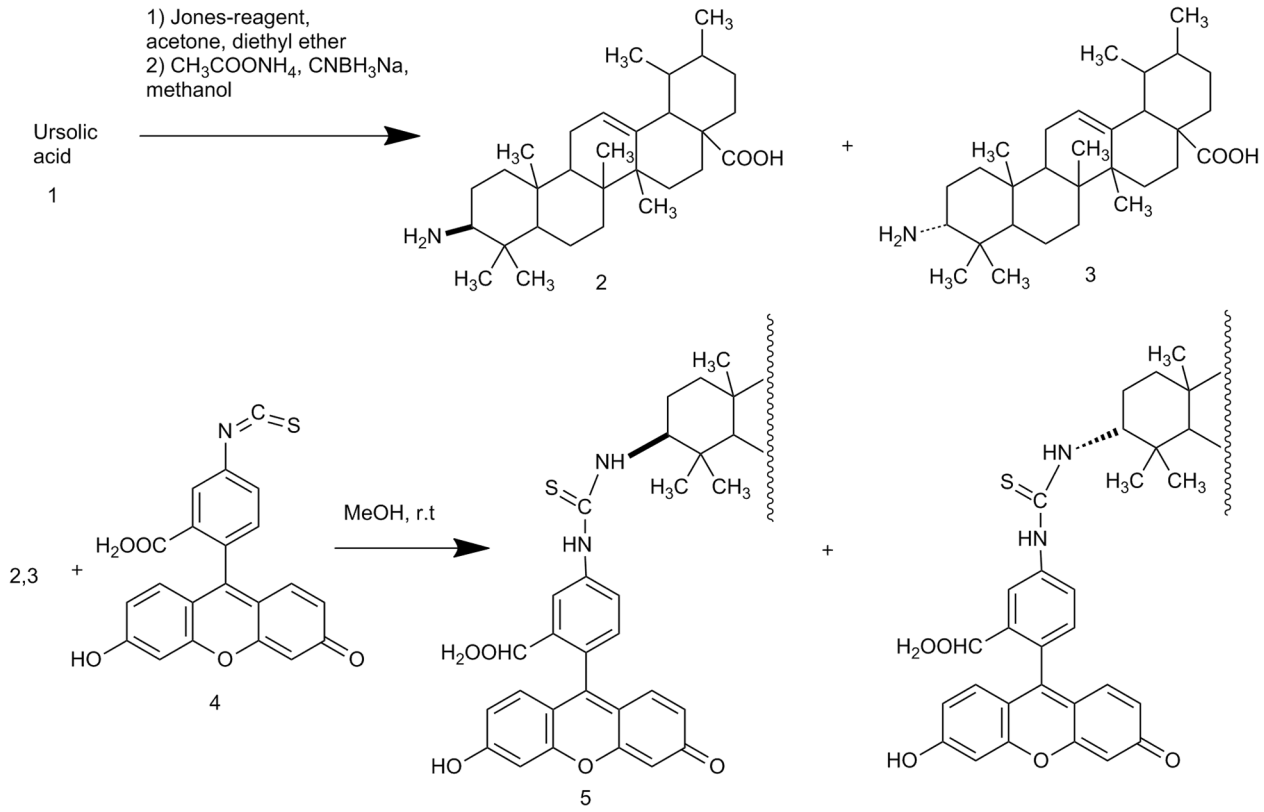

Fig. 2. The scheme for obtaining ursolic acid labeled with FITC.

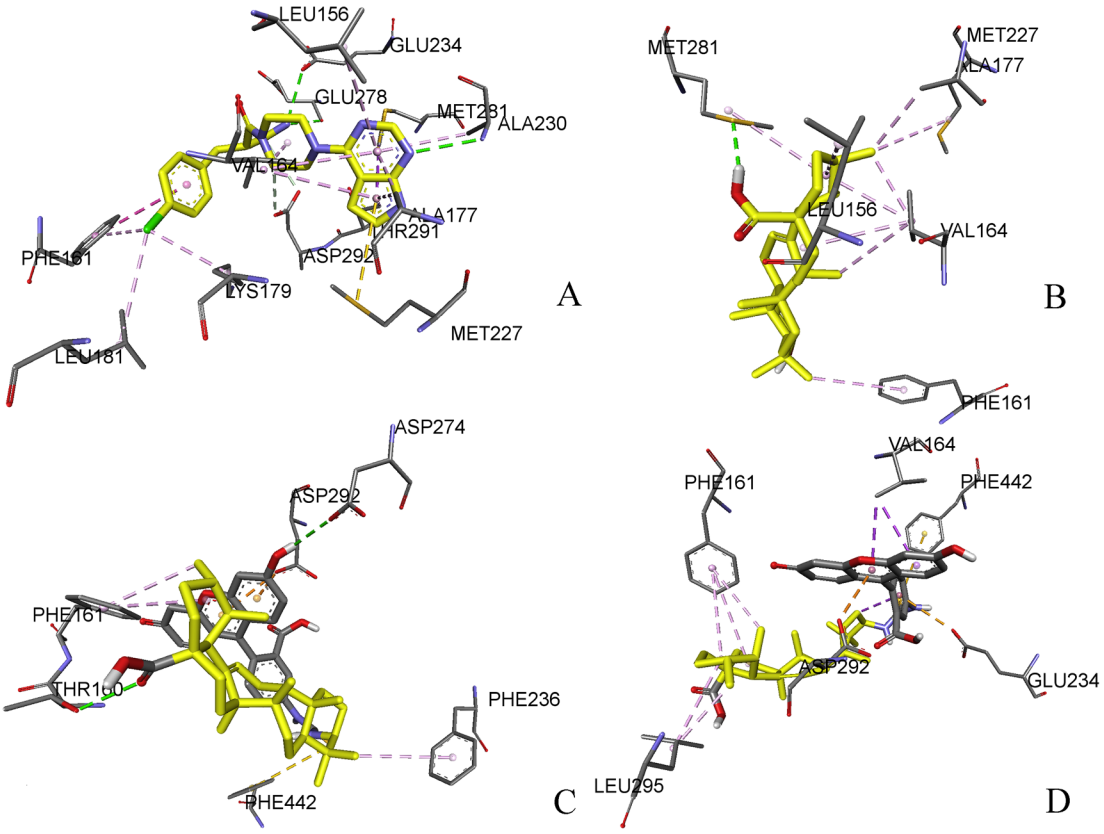

Fig. 3. Interaction between ligands and Akt1: (A) referent ligand XM1; (B) ursolic acid; (C) α-epimer; (D) β-epimer. Non-covalent interactions are shown as dashed lines: hydrogen bonds – green, hydrophobic interactions – purple, ionic interactions – orange. In ligands, ursolic acid is shown in yellow, FITC part of molecule is gray.

urs-12(13)-en-28-oic acid is the reaction of the epimers **2** and **3** with fluorescein isothiocyanate **4**, which proceeds under mild conditions at room temperature, resulting in products **5** and **6** with yields of 88 and 82% respectively. It should be noted that, despite the starting materials being widely-known, the synthesized products have not previously been described.

2. Results and discussion

2.1. Molecular modeling and molecular dynamics simulations for ursolic acid and its FITC labeled epimers

Previously, we have reported on a proposed mode of action of pentacyclic triterpene acids, where we suggested that Akt1/protein kinase B and MDM2/E3 ubiquitin-protein ligase were their binding targets [32]. In order to test this hypothesis we suggested a new approach, based on fluorescent labeling of the compounds under test, and chose ursolic acid as the modeling compound.

We performed a molecular docking, which allowed us to estimate the binding energy between the protein macromolecule and the potential ligand and to draw conclusions on whether an interaction was likely, in order theoretically, to substantiate the idea that binding would still continue after the addition of the label.

Docking was performed for ursolic acid and its fluorescent labeled epimers. The binding energies are shown in Table 1. The results are visualized in Figs. 3 and 4.

These results indicate that the interaction with Akt1 and MDM2 is preserved even after addition of the fluorescent label.

To determine the stability of the predicted conformations six protein–ligand complexes of ursolic acid and its FITC labeled epimers with Akt1 and MDM2 proteins were exposed to MD simulation.

The RMSD of the backbone atoms of each residue in complexes of UA, α-epimer and β-epimer with Akt1 and MDM2 was analyzed to observe the stability of the ligand/protein structure. The comparisons of the RMSD values of UA/Akt1, α-epimer/Akt1 and β-epimer/Akt1 complexes are shown in Fig. 5.

During the first 6.500 ps, the values for β-epimer/Akt1 complex are more variable and on average exceed the values for UA/Akt1 and α-epimer/Akt1 complexes. Then, up to 10.000 ps, the RMSD values and its variability for β-epimer/Akt1 complex are significantly reduced. The α-epimer/Akt1 complex is generally more stable than UA/Akt1, but after 8000 ps of MD simulation the values of its RMSD converge. Thus, it should be assumed that α-epimer/Akt1 complex is more stable than β-epimer/Akt1. The presence of β-epimer leads to significant fluctuations in the backbone structure of the Akt1 protein.

The RMSD values of UA/MDM2, α-epimer/MDM2 and β-epimer/MDM2 complexes are shown in Fig. 6.

The UA/MDM2 complex is the most unstable - high variability of RMSD value is observed. During the first 3.000 ps, FITC labeled epimers complexes exhibit a similar stability pattern. However, then the average value of RMSD for β-epimer /MDM2 complex increases, while the variability and average value of RMSD for α-epimer/MDM2 complex becomes the lowest. The most stable complex is α-epimer/MDM2.

2.2. Synthesis of fluorescent labeled epimers

After molecular modeling a synthesis to obtain labeled epimers was performed. The following show the structures of the obtained ursolic acid epimers and of FITC (Figs. 7 and 8).

The products at each stage of synthesis were characterized by NMR-analysis. An elemental analysis was conducted, confirming the appropriate ratio of the elements in the above structural formulae.

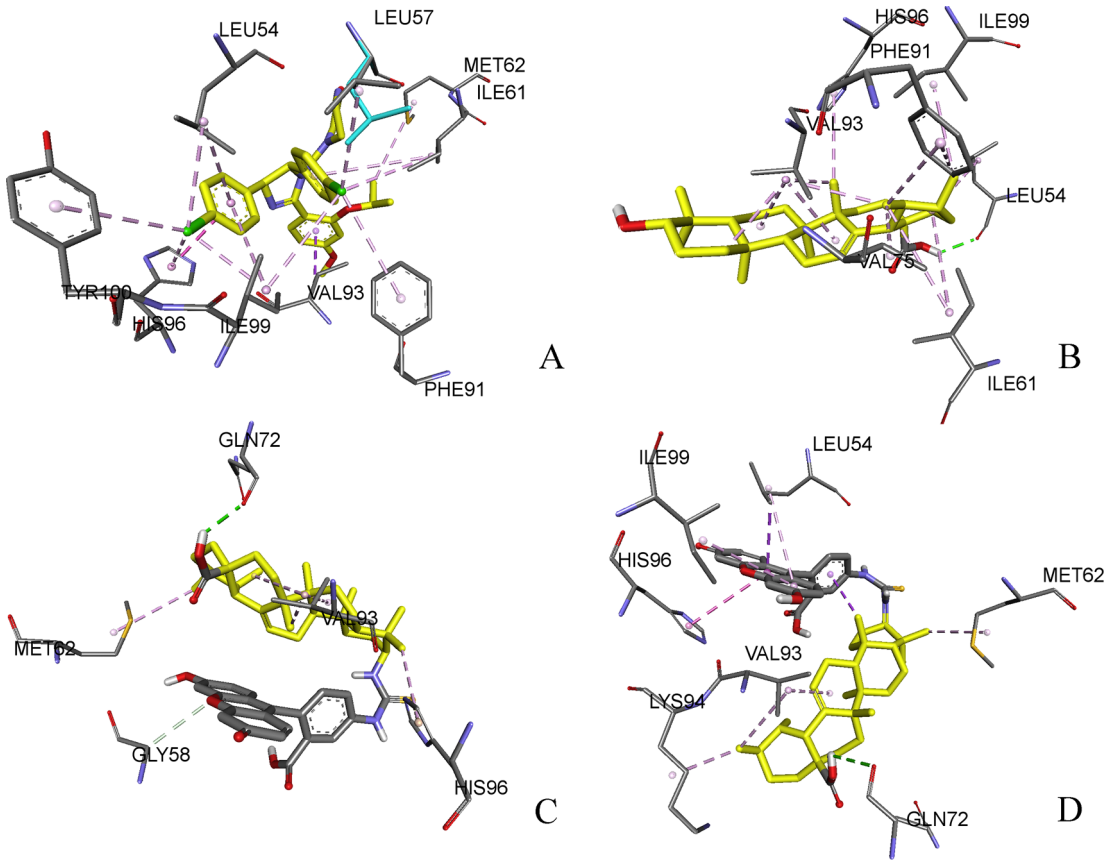

Fig. 4. Interaction between ligands and MDM2: (A) referent ligand Nutlin 3a; (B) ursolic acid; (C) α-epimer; (D) β-epimer. Non-covalent interactions are shown as dashed lines: hydrogen bonds – green, hydrophobic interactions – purple. In ligands, ursolic acid is shown in yellow, FITC part of molecule is gray.

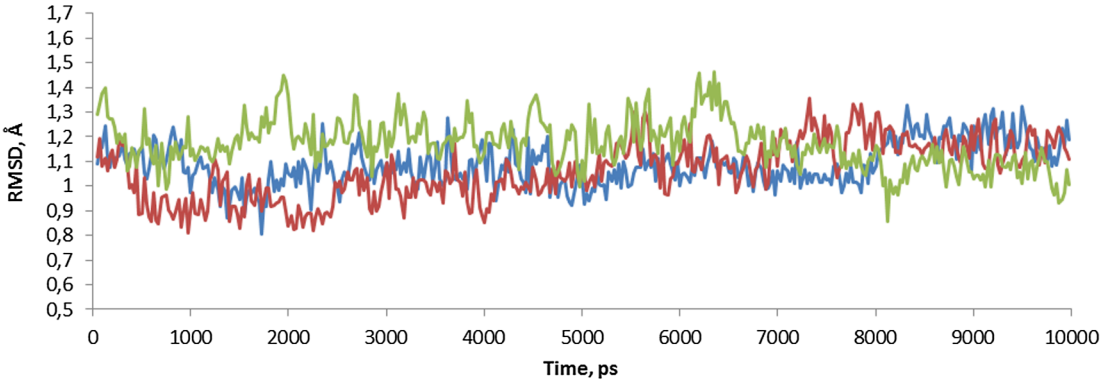

Fig. 5. RMSD of the backbone atoms of Akt1 docked complexes at 300 K. Complexes are indicated: blue – UA/Akt1, red – α-epimer/Akt1, green – β-epimer/Akt1.

2.3. Investigation of cytotoxic activity

The next stage was to check the changes in properties under *in vitro* conditions. For this, an MTT-assay was carried out for ursolic acid. Data are summarized in Table. 2.

Then, using the same technique, the cytotoxic properties of the resulting conjugate was checked. The ratio of label was varied from 0 to 100%, the other fraction being native ursolic acid. The total concentration of the compounds was 50 μM in all cases (Fig. 9).

During the *in vitro* experiments we demonstrated that adding the label intensifies the cytotoxic properties of ursolic acid, but there was a more pronounced effect with the β-epimer (UA*) and so this was then examined in greater detail with cells from the MCF-7 line. As this line has been thoroughly studied, including the effects of treatment with triterpene compounds, this allowed us to make a full comparison of our results with the available data.

2.4. Detection of apoptosis

Apoptosis was detected with acridine orange/ethidium bromide double staining, 24 and 48 h after the treatment of the MCF-7 cells with the labeled ursolic acid at a concentration of 25 μM. The results are shown in Table 3, Fig. 10.

2.5. Investigation of cell morphology using the cell IQ system

As indicated above, the addition of the label intensifies the apoptotic properties of the ursolic acid. A detailed examination of the dynamics of the cytotoxic effect of UA* was made visually using the Cell IQ system. Cell death was detected 3 h after the start of incubation (the

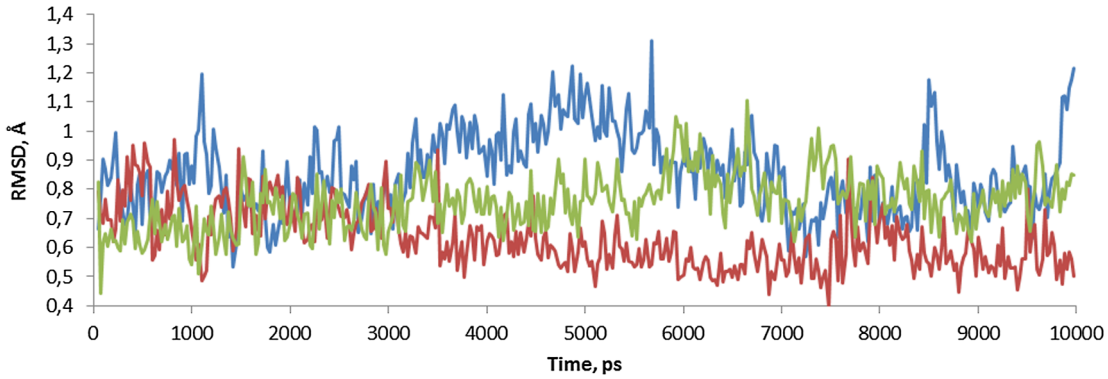

Fig. 6. RMSD of the backbone atoms of MDM2 docked complexes at 300 K. Complexes are indicated: blue – UA/MDM2, red – α-epimer/MDM2, green – β-epimer/MDM2.

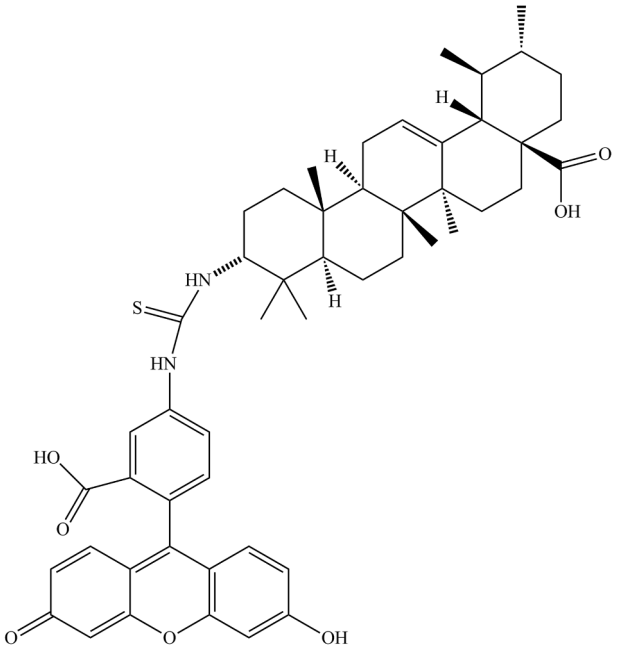

Fig. 7. α-Epimer of ursolic acid labeled with FITC.

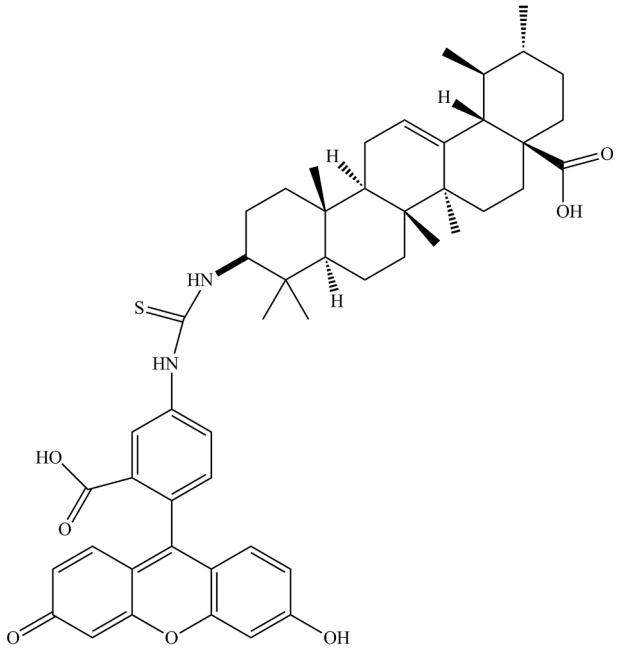

Fig. 8. β-Epimer of ursolic acid labeled with FITC.

cells became rounded, detached from the surface and fragmented). At the end of the experiment almost all the cells were dead. The results are shown in Table 4.

Also using Cell IQ, we chose a duration (the first 24 h of incubation) that would enable a more detailed examination of cell morphology, using confocal microscopy.

Table 2
Half-maximal inhibitory concentration (IC_{50}) for ursolic acid after 72 h of incubation.

Cell line	IC_{50}, μM
human lymphocytes	90.89 ± 5.5
MCF-7	25.05 ± 3.17*

* p-Value ≤ 0.01, compared with the control group.

2.6. Confocal microscopy

We carried out microscopical analysis of MCF-7 line cells treated with the β-epimer. The cells were examined over the first 24 h after treatment, at intervals of 3 h, and by 24 h there was a significant, visible, apoptotic effect. To define the changes in cell morphology we used additional stains: DAPI, CellMask Orange and MitoTracker Red. Such a combination allowed us to identify the changes in structures of the plasmalemma, the inner membranes, the mitochondria and the nuclei. The results of confocal fluorescence microscopy are shown in Table 5.

The appearance of a labeled ursolic acid signal in the MCF-7 line cells was registered 6 h after the treatment; the signal intensified as time went on. After 12 h of incubation with labeled ursolic acid its signal distribution visually overlapped with the signal from the CellMask Orange stain, leading us to infer that the label was located on the inner membranes (EPR, Golgi apparatus, and endosomes). After 18 h the labeled ursolic acid signal localization started to coincide with the MitoTracker Red, suggesting that the preparation was binding with mitochondrial receptors. Finally, after 24 h the signal could be identified not only associated with the inner membranes and mitochondria, but also within the nucleus. Image processing with Zen (Carl Zeiss) software visualized overlapping of the signals from the labeled ursolic acid, CellMask Orange and MitoTracker Red, which confirmed their colocalization (Figs. 11, 12).

We have performed a model experiment to obtain labeled ursolic acid and to study its biological activity. The aim of this was to test the effectiveness of a new approach for studying the mechanism of the cytotoxic effect of the ursane series of pentacyclic triterpenic acids.

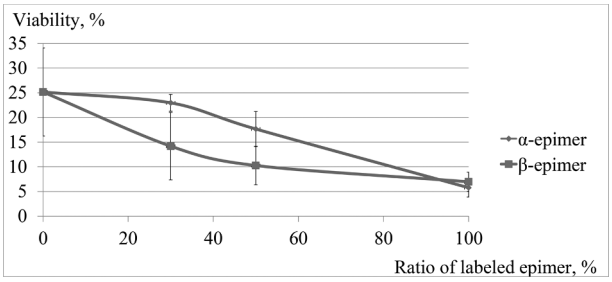

Fig. 9. Investigation of the cytotoxic properties of ursolic acid labeled with FITC on the MCF-7 cell line. The ratio of label was varied from 0 to 100%, the other fraction being native ursolic acid. The total concentration of the compounds was 50 μM in all cases.

Table 3
Apoptosis stages (%) of MCF-7 cell line treated with ursolic acid and UA* at 25 μM after 48 and 72 h of incubation.

24 h			
	Normal cells	Apoptosis	Necrosis
Control	96.8 ± 5.0	1.6 ± 0.1	1.6 ± 0.3
Ursolic acid	87.7 ± 11.1*	10.5 ± 2.0**	1.8 ± 0.2*
UA*	70.6 ± 10**	26.5 ± 5.3**	2.9 ± 0.3**
48 h			
Control	97.4 ± 6.2	1.3 ± 0.2	1.3 ± 0.2
Ursolic acid	78.7 ± 12.3**	16.4 ± 3.1**	4.9 ± 0.6**
UA*	69.5 ± 8.8**	25.6 ± 4.3**	4.9 ± 0.7**

* p-Value ≤ 0.05.
** p-Value ≤ 0.01 compared with the control group.

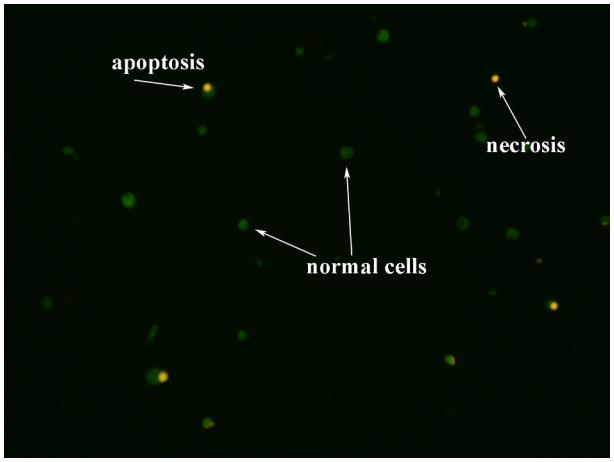

Fig. 10. Investigation of proapoptotic activity of UA* on MCF-7 cell line. Normal cells are colored green with acridine orange, at apoptosis the cell nucleus is coloured red with ethidium bromide, and the cytoplasm is coloured green with acridine orange. Dead cells are stained only with ethidium bromide.

Ursolic acid has been shown to be capable of causing apoptosis both externally in its association with the cellular membranes, and by action on the mitochondria [33–36]. It is also capable of suppressing the growth of cancerous cells through mobilization of AMP-activated protein kinase [37]. We found out that ursolic acid can also initiate another type of programmed cell death – autophagy, and thus it can inhibit the growth of cancer cells [38,39]. However, there is evidence from experiments on PC3 cancer cells of the prostate gland that suggests autophagy could be considered to be a cell defense reaction to the induction of apoptosis by ursolic acid [40]. Adding autophagy inhibitors intensified the apoptosis. As a result, of this work the authors conclude that if ursolic acid is to be used as an anti-neoplastic agent, it is necessary to add autophagy inhibitors.

With the help of bioinformatic approaches we predicted a number of targets, in particular, Akt1 and MDM2, for the ursolic acid [7,41–43]. There is other experimental data that has demonstrated the impact of ursolic acid on these proteins [34,44]. In the cell, Akt1 is localized mostly on the inner membranes [45], while MDM2 is located in the nucleoli [46,47]. Experimental tracing of the dynamics of penetration and distribution of the labeled ursolic acid has shown that when the acid enters the cell, it initially localizes on the inner membranes where the predicted target Akt1 – a protein that inhibits apoptosis – is located. Its inhibition by ursolic acid may induce apoptosis in the cancerous cells, followed by breaching of the mitochondrial membrane and the integrity of the cell nucleus. The signal present in the mitochondria 18 h after treatment may witness that they are vulnerable to the labeled ursolic acid because of the developing apoptotic changes in the cell. However, such an assumption is not exclusive of the possibility that these membranes may have their own targets for the compound being tested, but these were not included in the scope of this research. The penetration of the label into the nucleus after 24 h may be interpreted as an integrity breach of the nuclear membrane of the type that is typical of apoptosis. We found no localization of labeled ursolic acid typical of binding with nucleoli: the signal was equidistributed across the nucleus, which indirectly evidences a lack of interaction between the labeled ursolic acid and MDM2. The results obtained are in agreement with, and complement, the available data.

3. Experimental section

3.1. Molecular docking and dynamics

The macromolecules and ligands were prepared with the use of the UCSF Chimera 1.10.2 software program [48], the structure of the ursolic acid was obtained from the PubChem database (CID 64945). We used the MMFF94 force field to obtain their three-dimensional structures [49]. The molecular docking was performed in AutoDock Vina [50] using the PyRx 0.8 graphical interface. In order to visualize the results, Accelrys Discovery Studio Visualizer 4.0 software was used.

As potential targets for the triterpenic acids we chose Akt1/protein kinase B (PDB ID: 3OCB) [51] and MDM2/ E3 ubiquitin-protein ligase (PDB ID: 4HG7) [52] (referent ligands were (2S)-2-(4-chlorobenzyl)-3-oxo-3-[4-(7H-pyrrolo[2,3-*d*]pyrimidin-4-yl)piperazin-1-yl]propan-1-amine (XM1) and 4-({(4S,5R)-4,5-bis(4-chlorophenyl)-2-[4-methoxy-2-(propan-2-yloxy)phenyl]-4,5-dihydro-1H-imidazol-1-yl}carbonyl)piperazin-2-one (nutlin 3a) respectively). The docking procedure was performed with the use of standard AutoDock Vina parameters using a strict conformation of the macromolecule but a flexible conformation of the ligand. The conformations with the lowest values of minimal binding energy from the point of view of evaluating the docking function have been chosen for the visualization.

Molecular dynamics simulations were performed using the NAMD 2.13 package [53]. Ligand-enzyme complexes with the lowest binding energy were selected for MD. The ligand parameters were analyzed on the SwissParam online server [54] using MMFF [49] and CHARMM22 [55] forcefields. Complexes preparation, solvation, neutralization and analysis were carried out using VMD program [56]. Energy minimization was performed for 1000 steps using the steepest descent method [57]. The complexes were heated to 300 K and equilibrated at the NVT ensemble for 100 ps at 300 K. Finally, 10 ns MD simulations were performed at the NPT canonical ensemble under periodic boundary conditions. The trajectory of each complex was analyzed using VMD RMSD Trajectory Tool.

3.2. Synthesis of ursolic acid labeled with FITC

The ursolic acid used was manufactured by Aldrich, and the FITC, by Fluka. All other reagents were purchased from ReaChem, class CP

Table 4
Investigation of the morphology of MCF-7 cells treated with ursolic acid and UA* at a concentration of 25 μM using the Cell-IQ system during 72 h of incubation.

Time, h	Ursolic acid	UA*
0	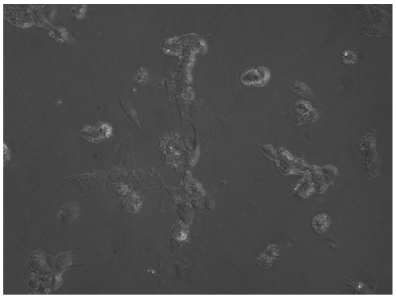	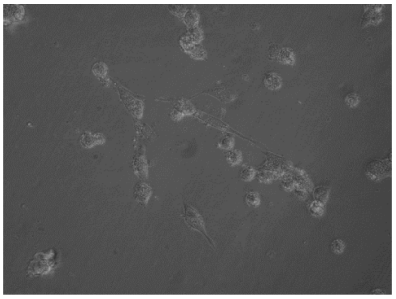
3	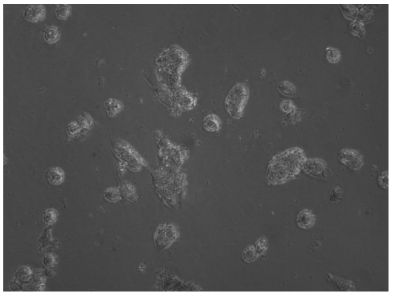	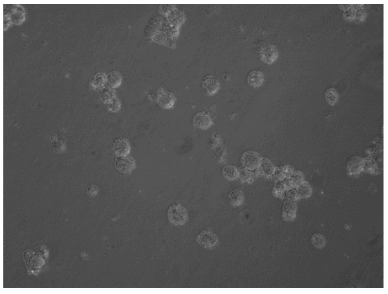
24	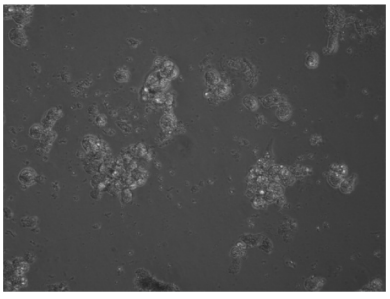	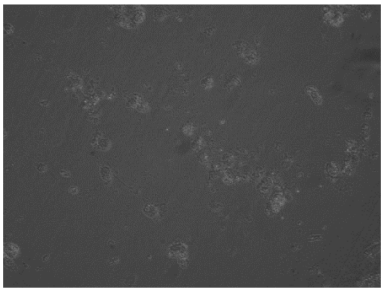
48	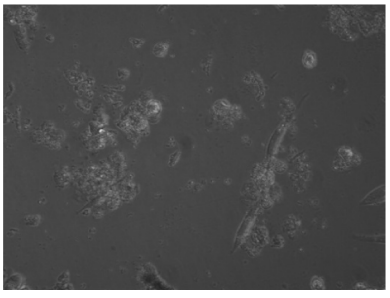	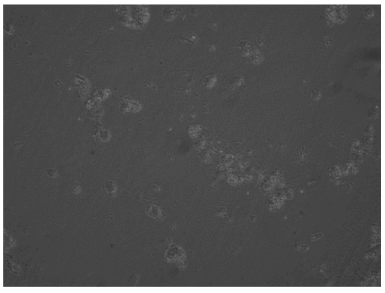
72	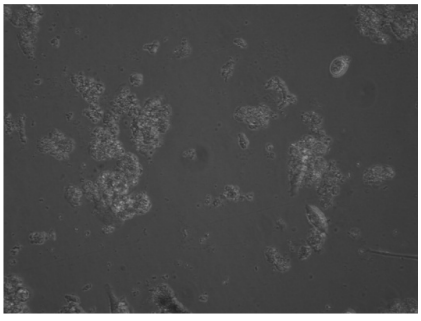	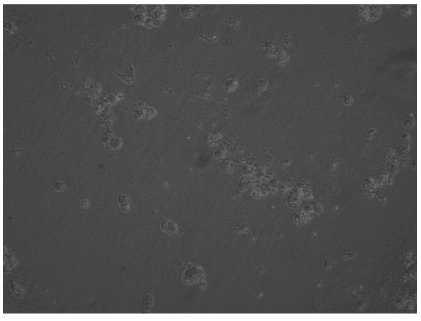

(Chemically Pure).

The NMR-spectra were obtained with a Bruker AV-400 (1H: 400.13 MHz, 13C: 100.78 MHz) or Bruker AV-600 spectrometer (1H: 600.30 MHz, 13C: 150.95 MHz) (Bruker BioSpin GmbH, Rheinstetten, Germany), using tetramethyl silane as the external standard. The melting points were determined on a Stuart SMF-38 (Bibby Scientific, Staffordshire, UK). The elemental analysis was carried out with the use of a Carlo-Erba analyzer (Carlo-Erba, Milan, Italy). The reaction progress was monitored using TLC on Siluf l UV-254 plates (Kavalier, Czech Republic), the chromatographic separation being carried out on

Table 5
Analysis of distribution of UA* in MCF-7 cells carried out with confocal fluorescence microscopy.

Time, h	DAPI + UA* + CellMask Orange	DAPI + UA* + MitoTracker Red
3	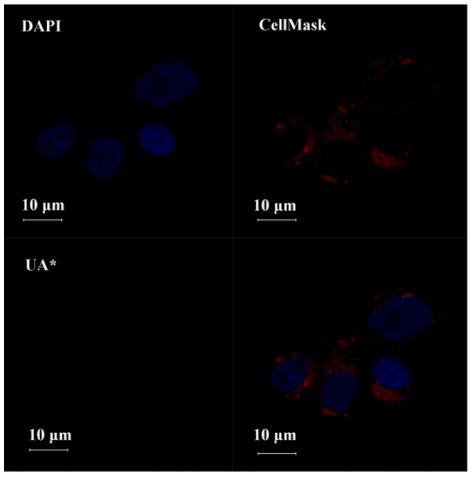	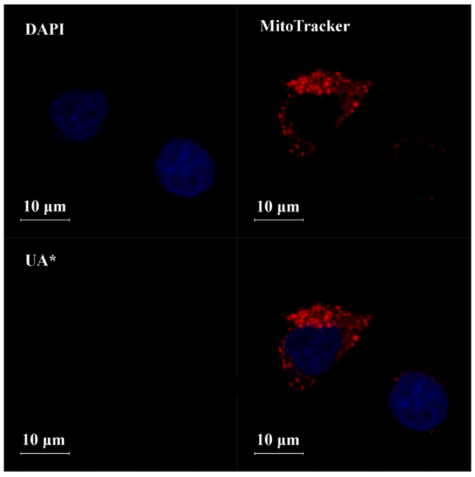
6	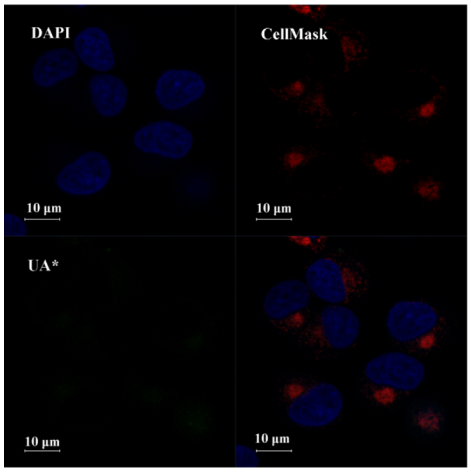	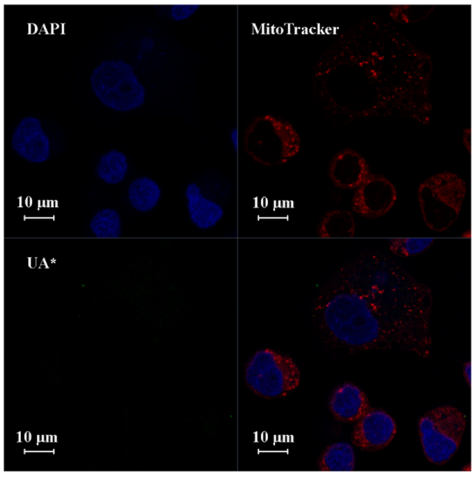
12	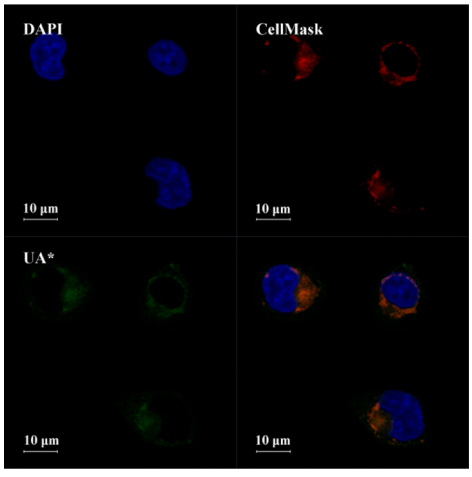	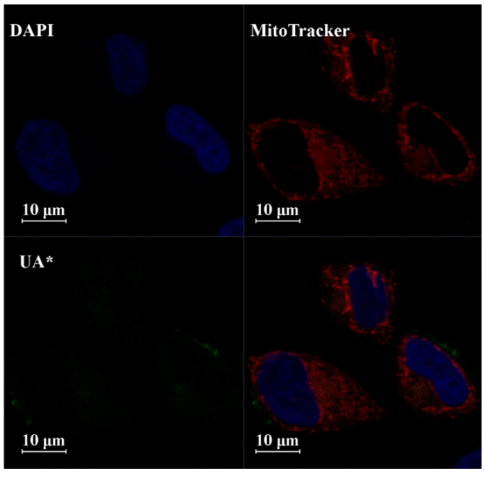

(*continued on next page*)

Table 5 (*continued*)

Time, h	DAPI + UA* + CellMask Orange	DAPI + UA* + MitoTracker Red
18	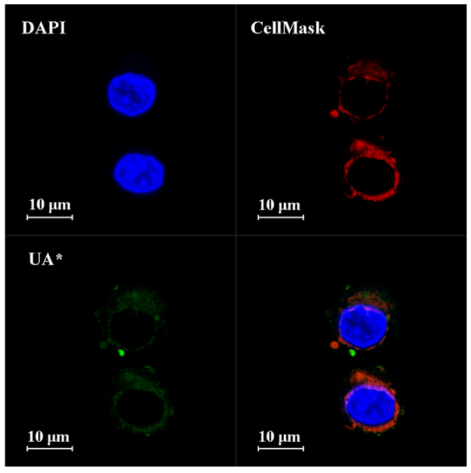	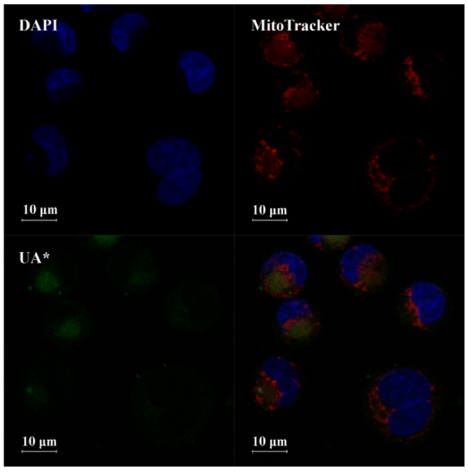
24	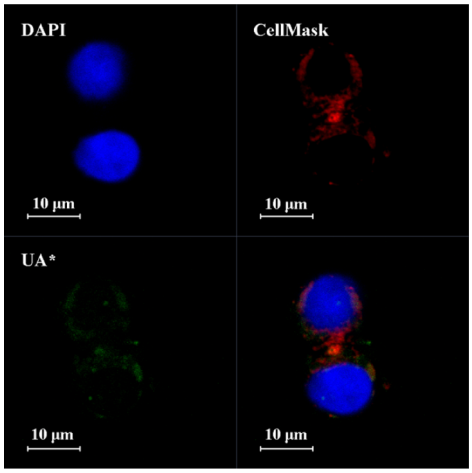	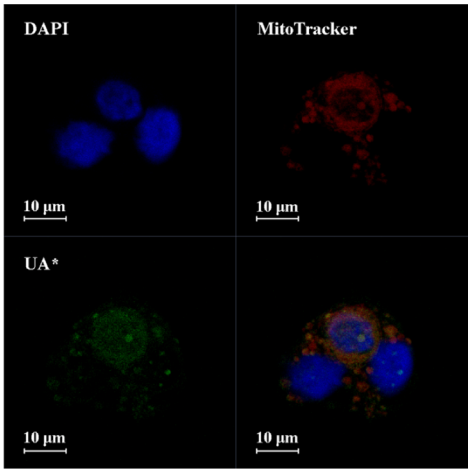

silica gel 60 (0.063–0.200 mm, Merck KGaA, Darmstadt, Germany). The epimers of 3α- and 3β-amino-urs-12(13)-en-28-oic acid **2** and **3** were prepared according to established technique; their spectral data completely corresponding to the data stated in the paper [30].

Compounds **5** and **6** were obtained by reacting the corresponding epimers: (20 mg (0.04 mM)) to 10 ml of methanol we added 17 mg of fluorescein isothiocyanate **4** and stirred the solution for 12 h at room temperature in the dark. Then the solution was evaporated under vacuum, and the residue further dried. We obtained the products **5** and **6** with yields of 88 and 82% respectively.

α-10-(3-(3-Carboxy-4-(6-hydroxy-3-oxo-3H-xanthen-9-yl) phenyl)thioureido)-1,2,6a,6b,9,9,12a-heptamethyl-1,2,3,4,4a,5,6,6a,6b,7,8,8a,9,10,11,12,12a,12b,13,14b-icosahydropicene-4a-carboxylic acid 5. Yield 88%. white powder. Rf 0.33 (hexan: methyl tert butyl ether 5:1) M.p. 259–2600C (diethylic ether). IR, ν, cm^{-1}: 3400, 3234, 3068, 2927, 2871, 2618, 2113, 2028, 1731, 1695, 1635, 1606, 1525, 1506, 1457, 1378, 1311, 1295, 1255, 1209, 1178, 1112, 1081, 1035, 995, 852. 1H NMR (CDCl3 + CD3OD, 400 MHz) δ 0.65 (3H, s, Me-25), 0.78 (3H, s, Me-26), 0.80 (3H, s, Me-27), 0.90 (3H, s, Me-24), 1.07 (3H, s, Me-23), 1.56 (3H, s, Me-30), 1.89 (1H, m, H33), 2.35 (1H, m, H19), 5.44 (4H, m, H31, H29), 5.65 (s, 1H, H18′), 6.90 (d, 1H, H12′), 7.44, 7.47 (s, 2H, H11′,H5′), 7.49 (d, 1H, ,H21′), 7.72 (d, 1H, H4′), 7.95 (s, 1H, H14′), 8.13 (s, 1H, H8′), 8.87 (d, 1H, H20′). 13C NMR (CDCl3 + CD3OD, 100 MHz) δ 15.04, 16.42, 17.83, 20.48, 22.94, 23.72, 26.19 (7*CH3 23,24,25,26,27,29,30), 19.19 (C6), 22.78 (C11), 23.62 (C16), 26.21 (C15), 27.48 (C2), 28.19 (C21), 30.16 (C7), 32.59 (C22), 35.89 (C19), 36.36 (C1), 38.20 (C10), 38.50 (C8), 38.66 (C20), 39.00 (C14), 46.64 (C17), 47.11 (C4), 48.93 (C9), 52.40 (C5), 54.85 (C18), 102.01 (C8′), 112.29 (C6′), 116.25 (C10′), 121.55 (C2″), 124.61 (C4a′), 125.07 (C12), 127.31 (C3″), 127.38 (C4″), 127.72 (C1″), 128.22 (C3′), 128.69 (C2′), 129.07 (C5″), 130.64 (C5′), 137.74 (C6″), 140.29 (C4′), 143.37 (C13), 145.37 (C3a′), 159.67 (C7′), 159.84 (C9a′), 160.20 (C3), 160.36 (C8a′), 171.28 (C7″), 179.19 (C28), 180.16 (C1′), 189.15 (NH═(C═S)═NH). Anal. calcd. for C51H60N2O7S C(72.48%) H(7.16%) N(3.31%) S(3.79%) found C(72.16%) H(6.93%) N(3.22%) S(3.60%). MS *m/z* calcd. 845.0963 found 845.1144

β-10-(3-(3-carboxy-4-(6-hydroxy-3-oxo-3H-xanthen-9-yl) phenyl)thioureido)-1,2,6a,6b,9,9,12a-heptamethyl-1,2,3,4,4a,5,6,6a,6b,7,8,8a,9,10,11,12,12a,12b,13,14b-icosahydropicene-4a-carboxylic acid 5. Yield 82%. white powder. Rf 0.31 (hexan: methyl tert butyl ether 5:1) M.p. 229–2300C (diethylic ether). IR, ν, cm^{-1}: 3413, 3403, 3111, 3025, 2917, 2870, 2628, 2110, 2008, 1731, 1695, 1635, 1604, 1524, 1506, 1437, 1375, 1311, 1295, 1245, 1207, 1178, 1112, 1081, 1035, 995, 852. 1H NMR (CDCl3 + CD3OD, 400 MHz) δ 0.68 (3H, s, Me-25), 0.74 (3H, s, Me-26), 0.80 (3H, s, Me-27), 0.89 (3H, s, Me-24), 1.01 (3H, s, Me-23), 1.54 (3H, s, Me-30), 1.85 (1H, m, H33), 2.34 (1H, m, H19), 5.41 (4H, m, H31, H29), 5.68 (s, 1H, H18′), 6.90 (d, 1H, H12′), 7.42, 7.47 (s, 2H, H11′,H5′), 7.48 (d, 1H, ,H21′), 7.65 (d, 1H, H4′), 8.01 (s, 1H, H14′), 8.18 (s, 1H, H8′), 8.82 (d, 1H, H20′). 13C NMR (CDCl3 + CD3OD, 100 MHz) δ 15.06, 16.44, 17.35, 20.39, 22.92, 23.72, 26.19 (7*CH3 23,24,25,26,27,29,30),

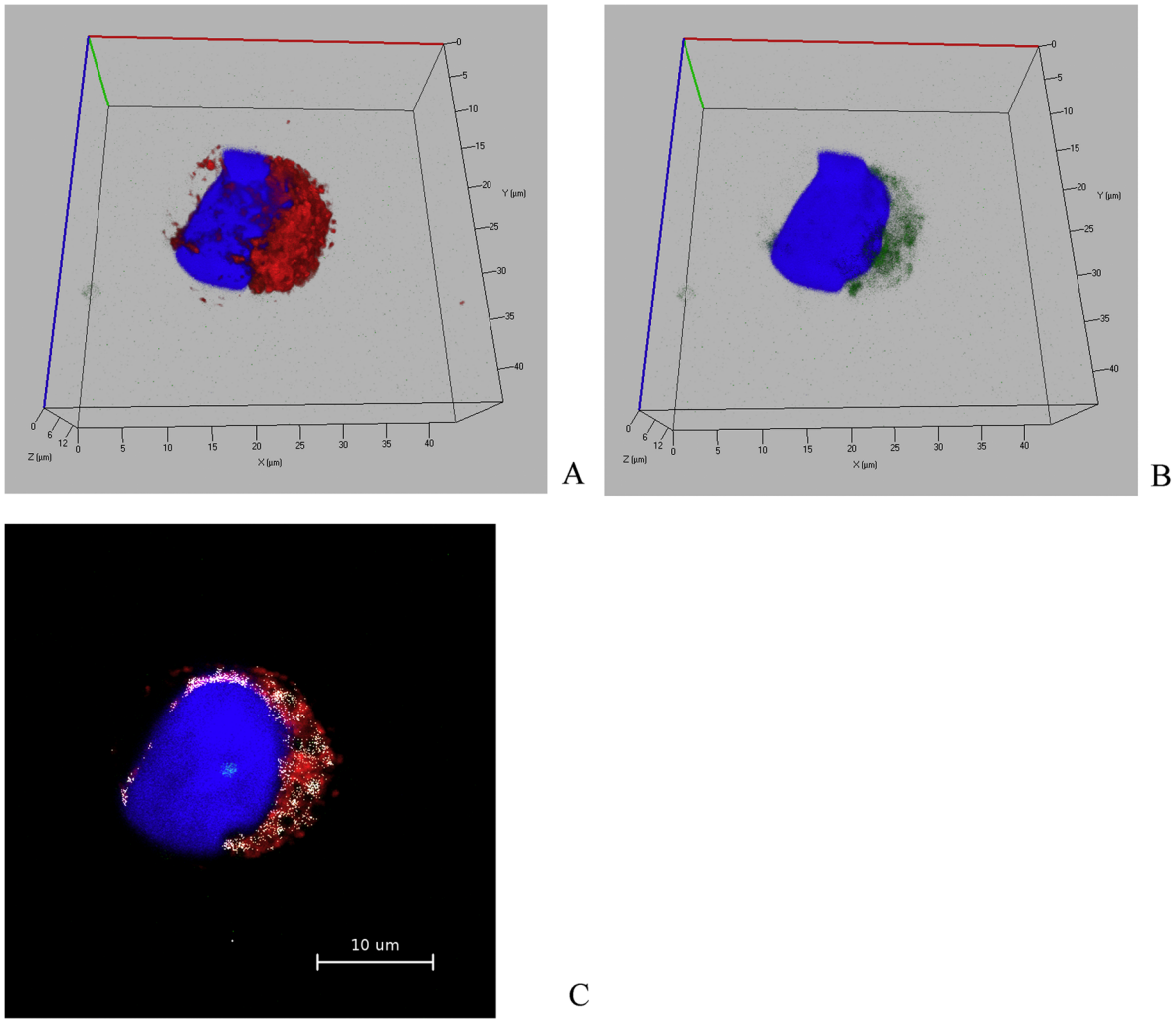

Fig. 11. Signal colocalization of UA* and CellMask in MCF-7 cells after 24 h of incubation: (A) 3D visualization of CellMask distribution; (B) 3D visualization of UA* distribution; (C) merged 2D visualization, white color marks overlapping signals from UA* and CellMask Orange. The nuclei are colored with DAPI.

19.20 (C6), 22.75 (C11), 23.60 (C16), 26.21 (C15), 27.48 (C2), 28.19 (C21), 30.14 (C7), 32.55 (C22), 35.89 (C19), 36.32 (C1), 38.46 (C10), 38.51 (C8), 38.60 (C20), 39.00 (C14), 46.62 (C17), 47.11 (C4), 49.03 (C9), 52.41 (C5), 54.80 (C18), 102.03 (C8′), 112.29 (C6′), 116.25 (C10′), 121.46 (C2″), 123.61 (C4a′), 125.06 (C12), 127.13 (C3″), 127.38 (C4″), 127.65 (C1″), 128.12 (C3′), 128.69 (C2′), 129.07 (C5″), 130.63 (C5′), 137.74 (C6″), 140.26 (C4′), 143.17 (C13), 145.35 (C3a′), 159.67 (C7′), 159.84 (C9a′), 160.21 (C3), 160.34 (C8a′), 171.25 (C7″), 179.19 (C28), 180.16 (C1′), 188.97 (NH═(C═S)═NH). Anal. calcd. for C51H60N2O7S C(72.48%) H(7.16%) N(3.31%) S(3.79%) found C(72.36%) H(7.13%) N(3.46%) S(3.30%). MS *m/z* calcd. 845.0963 found 845.1085.

3.3. MTT-assay

MTT-assay was performed according to standard procedures [58]. The cell cultures were grown on IMDM (with 3.02 g $NaHCO_3$ per liter of medium) containing 10% bovine serum. To each well of a 96-well plate we added 100 µl of the cell suspension (density 10^6 cells per ml); the plate was placed in an incubator containing 5% CO_2 at a temperature of 37 °C. After 24 h the test compounds were added at 1 µl per well. The plate was then returned to the incubator for a further 72 h. Then, 10 µl of MTT (5 mg of 3-(4,5-dimethylthiazol-2-yl)-2,5-diphenyltetrazolium bromide (MTT) per 1 ml of PBS) was added to each well. 3 h later the supernatant fluid was removed from the wells, and the precipitate was dissolved in 100 µl of isopropanol. The amount of precipitate was determined on a Multiskan RC plate spectrophotometer, using the inbuilt Genesis software (LabSystems). Percent inhibition was calculated by the formula:

$$\text{Inhibition } (\%) = 100 - -[(T/M) \times 100],$$

T is the optical density of the precipitate with the test compound, M is the optical density of the precipitate with DMSO (used as a solvent, negative control). The experiment was repeated independently three times, with 3 replications in each. Average values were reported for all repeated experiments; the data were analyzed for significance using Wilcoxon rank test.

3.4. Detection of apoptosis

Detection of Apoptosis was carried out using double staining with acridine orange/ethidium bromide. Into a 12-well plate we added 1 ml of cells in culture medium (density 10^6 cells per ml). This was incubated for 24 h to allow adhesion, and then treated with the test compounds. Assays were carried out at 24 and 48 h using standard procedures [59] with subsequent analysis on an Axio Observer (Carl Zeiss) microscope. The experiment was repeated independently three times, with 3 replications in each. Average values were reported for all repeated experiments; the data were analyzed for significance using Wilcoxon rank test.

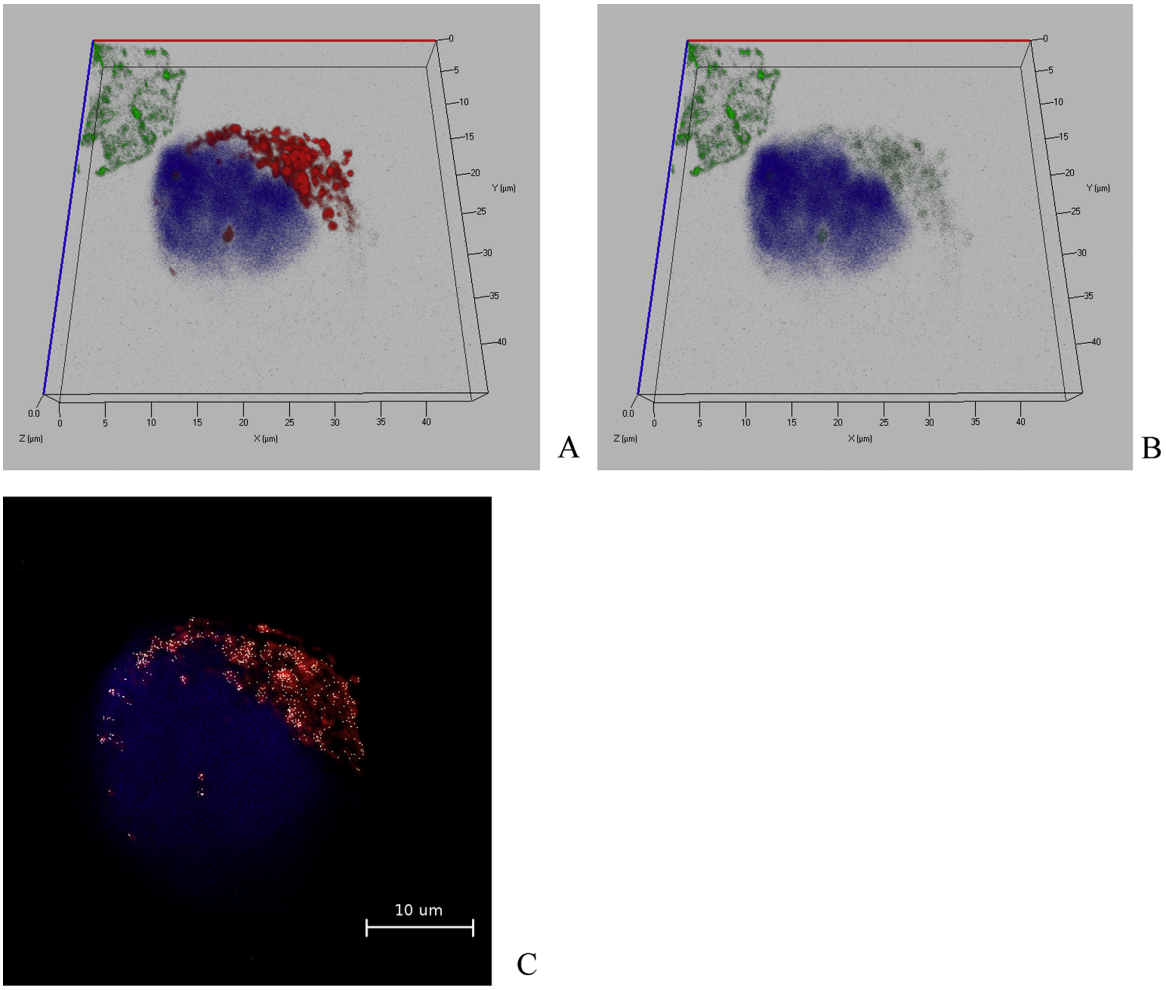

Fig. 12. Signal colocalization of UA* and MitoTracker Red in MCF-7 cells after 24 h of incubation: (A) 3D visualization of MitoTracker Red distribution; (B) 3D visualization of UA* distribution; (C) merged 2D visualization, white color marks overlapping signals from UA* and MitoTracker Red. The nuclei are colored with DAPI.

3.5. Cell IQ system

A Cell IQ System (CM Technologies, Finland) was used for *in vivo* observation of the cells over a 72 h period with a recording frequency of 6 images per hour. The cultures were grown in IMDM (with 3.02 g of $NaHCO_3$ per liter of medium) containing 10% bovine serum. 100 µl of the cell suspension (density 10^6 cell per ml) was placed into each well of a 96-well plate and this was then incubated at 37 °C in 5% CO_2. 24 h later the test compounds were added at 1 µl per well. The plate was then placed into the Cell-IQ system for 72 h, with cell imaging being recorded every 10 min, using a Nikon CFI Plan Fluorescence DL 10x objective lens.

3.6. Confocal microscopy

The samples for confocal microscopy were prepared as follows: a cover slip was placed into the bottom of each well of a 12-well plate, 1 ml of cell culture medium and 100 µl of cell suspension (density 10^6 cell per ml) were then added to each well. The cells were incubated for 24 h, and then washed with PBS. After that, to each well was added a sample of one of the compounds under test, dissolved in cell culture medium at the desired concentration. After a predetermined time the cover slips were removed from the plate, carefully washed with PBS and put into paraformaldehyde overnight. Subsequently, each coverslip was placed on a slide with antifade containing DAPI. The sample was dried with filter paper and the edges of the coverslips were sealed to the slides with lacquer. Microscopic examination was carried out with the help of an LSM 510 META (Carl Zeiss) confocal scanning microscope at the Center for Microscopic Analysis of Biological Objects of the Institute of Cytology and Genetics SB RAS. used standard filters were used for detection of FITC labeled epimeres (490 nm for excitation and 525 nm for emission). The results were processed using Zen (Carl Zeiss) software.

Conflict of interest

The authors confirm that this article content has no conflict of interest.

Acknowledgements

The authors thank Dr. Alexander Baev for help with the MD similations, and the Center for Collective Use of Microscopic Analysis of Biological Objects (Institute of Cytology and Genetics, Siberian Branch of Russian Academy of Science, Novosibirsk, Russia) for providing the equipment.

The research was supported by the Program of Fundamental Research of the Siberian Branch of the Russian Academy of Sciences No. 0324-2018-0037.

References

[1] W.N. Setzer, M.C. Setzer, Plant-derived triterpenoids as potential antineoplastic

agents, Mini Rev. Med. Chem. 3 (2003) 540–556.
[2] N. Sultana, Clinically useful anticancer, antitumor, and antiwrinkle agent, ursolic acid and related derivatives as medicinally important natural product, J. Enzyme Inhib. Med. Chem. 26 (2011) 616–642.
[3] B.B. Aggarwal, Y. Takada, O.V. Oommen, From chemoprevention to chemotherapy: common targets and common goals, Exp. Opin. Investig. Drugs. 13 (2004) 1327–1338.
[4] D. Es-saady, A. Simon, M. Ollier, J.C. Maurizis, A.J. Chulia, C. Delage, Inhibitory effect of ursolic acid on B 16 proliferation through cell cycle arrest, Cancer Lett. 106 (1996) 193–197.
[5] P.O. Harmand, R. Duval, C. Delage, A. Simon, Ursolic acid induces apoptosis through mitochondrial intrinsic pathway and caspase-3 activation in M4Beu melanoma cells, Int. J. Cancer 114 (2005) 1–11.
[6] K.a. Manu, G. Kuttan, Ursolic acid induces apoptosis by activating p53 and caspase-3 gene expressions and suppressing NF-kB mediated activation of bcl-2 in B16F–10 melanoma cells, Int. Immunopharmacol. 8 (2008).
[7] W. Zhang, X. Men, P. Lei, Review on anti-tumor effect of triterpene acid compounds, J. Cancer Res. Ther. 10 (2014).
[8] K.-H. Sohn, H.-Y. Lee, H.-Y. Chung, H.-S. Young, S.-Y. Yi, K.-W. Kim, Anti-angiogenic activity of triterpene acids, Cancer Lett. 94 (1995) 213–218.
[9] C. Cárdenas, A.R. Quesada, M.Á. Medina, Effects of ursolic acid on different steps of the angiogenic processBiochem, Biophys. Res. Commun. 320 (2004) 402–408.
[10] P. Skopinski, J. Szaflik, B. Duda-Król, J. Nartowska, E. Sommer, J. Chorostowska-Wynimko, U. Demkow, E. Skopinska-Rózewska, Suppression of angiogenic activity of sera from diabetic patients with non-proliferative retinopathy by compounds of herbal origin and sulindac sulfone, Int. J. Mol. Med. 14 (2004) 707–711.
[11] C.-M. Ma, S.-Q. Cai, J.-R. Cui, R.-Q. Wang, P.-F. Tu, M. Hattori, M. Daneshtalab, The cytotoxic activity of ursolic acid derivatives, Eur. J. Med. Chem. 40 (2005) 582–589.
[12] H. Chen, Y. Gao, A. Wang, X. Zhou, Y. Zheng, J. Zhou, Evolution in medicinal chemistry of ursolic acid derivatives as anticancer agents, Eur. J. Med. Chem. 92 (2015) 648–655.
[13] Y.-Q. Meng, D. Liu, L.-L. Cai, H. Chen, B. Cao, Y.-Z. Wang, The synthesis of ursolic acid derivatives with cytotoxic activity and the investigation of their preliminary mechanism of action, Bioorg. Med. Chem. 17 (2009) 848–854.
[14] R. Weissleder, V. Ntziachristos, Shedding light onto live molecular targets, Nat. Med. 9 (2003) 123–128.
[15] M. Sameiro, T. Gonçalves, Fluorescent labeling of biomolecules with organic probes, Chem. Rev. 109 (2009) 190–212.
[16] C. Abate, J.R. Hornick, D. Spitzer, W.G. Hawkins, M. Niso, R. Perrone, F. Berardi, Fluorescenct derivatives of σ receptor ligand 1-cyclohexyl-4-[3-(5-methoxy-1,2,3,4-tetrahydronaphtalen-1-yl)propyl]piperazine (PB28) as a tool for uptake and cellular localization studies in pancreatic tumoe cells, J. Med. Chem. 54 (2011) 5858–5867.
[17] K.W. Crawford, W.D. Bowen, Sigma-2 receptor agonists activate a novel apoptotic pathway and potentiate antineoplastic drugs in breast tumor cell lines, Cancer Res. 62 (2002) 313–322.
[18] M.S. Ostenfeld, N. Fehrenbacher, M. Hoyer-Hansen, C. Thomsen, T. Farkas, M. Jaattela, Effective tumor cell death by σ-2 receptor ligand siramesine involves lysosomal leakage and oxidative stress, Cancer Res. 65 (2005) 8975–8983.
[19] H. Kashiwagi, J.E. McDunn, P.O. Simon, P.S. Goedegebuure, S. Vangveravong, K. Chang, R.S. Hotchkiss, R.H. Mach, W.G. Hawkins, Sigma-2 receptor ligands potentiate conventional chemotherapies and improve survival in models of pancreatic adenocarcinoma, J. Transl. Med. 7 (2009) 24.
[20] J. Levi, Z. Cheng, O. Gheysens, M. Patel, C.T. Chan, Y. Wang, M. Namavari, S.S. Gambhir, Fluorescent fructose derivatives for imaging breast cancer cells, Bioconjug. Chem. 18 (2007) 628–634.
[21] K.R. Barnes, J. Blois, A. Smith, H. Yuan, F. Reynolds, R. Weissleder, L.C. Cantley, L. Josephson, Fate of a bioactive fluorescent wortmannin derivative in cells, Bioconjug. Chem. 19 (2008) 130–137.
[22] J. Gertsch, F. Feyen, A. Bützberger, B. Gerber, B. Pfeiffer, K.-H. Altmann, Making epothilones fluoresce: design, synthesis, and biological characterization of a fluorescent N12-aza-epothilone (azathilone), Chembiochemistry 10 (2009) 2513–2521.
[23] C.L. Hartwig, E.M.W. Lauterwasser, S.S. Manajan, J.M. Hoke, R.A. Cooper, A.R. Renslo, Investigating the antimalarial action of 1,2,4-trioxolanes with fluorescent chemical probes, J. Med. Chem. 54 (2011) 8207–8213.
[24] J.a. Evangelio, M. Abal, I. Barasoain, A.a. Souto, M. Pilar Lillo, a. Ulises Acuña, F. Amat-Guerri, J.M. Andreu, Fluorescent taxoids as probes of the microtubule cytoskeleton, Cell Motil. Cytoskeleton 39 (1998) 73–90.
[25] J.F. Díaz, I. Barasoain, A.a. Souto, F. Amat-Guerri, J.M. Andreu, Macromolecular accessibility of fluorescent taxoids bound at a paclitaxel binding site in the microtubule surface, J. Biol. Chem. 280 (2005) 3928–3937.
[26] M. Izdebska, A. Klimaszewska-Wiśniewska, D. Lewandowski, J. Marcin Nowak, M. Gagat, A. Grzanka, Arsenic trioxide preferentially induces nonapoptotic cell deaths as well as actin cytoskeleton rearrangement in the CHO AA8 cell line, Postep. Hig Med. Dosw. 68 (2014) 1492–1500.
[27] S. Wu, N.J. Dovichi, High-sensitivity fluorescence detector fluorescein isothiocyanate derivatives of amino acids separated by capillary zone electrophoresis, J. Chromatogr. 480 (1989) 141–155.
[28] L. Fülöp, B. Penke, M. Zarándi, Synthesis and fluorescent labeling of beta-amyloid peptides, J. Pept. Sci. 7 (2001) 397–401.
[29] C. Hoffmann, J. Leroy-Dudal, S. Patel, O. Gallet, E. Pauthe, Fluorescein isothiocyanate-labeled human plasma fibronectin in extracellular matrix remodeling, Anal. Biochem. 372 (2008) 62–71.
[30] C.H. Brieskorn, H. Eschelbach, Glykamine von ursol- und 18P-glycyrrhetinsaure, Arch. Pharm. Res. 312 (1979) 752–762.
[31] K. Bowden, M. Heilbron, E.R.H. Jones, B.C.L. Weedon, Acetylenic ketones by oxidation of acetylenic carbinols and glycols, J. Chem. Soc. (1946).
[32] T.S. Frolova, A.V. Lipeeva, D.S. Baev, Y.A. Tsepilov, O.I. Sinitsyna, Apoptosis as the main mechanism of the cytotoxic action of ursolic and grind acids in glioma cells, Phytochem. Lett. 51 (2017) 61–68.
[33] K.H. Kim, H.S. Seo, H.S. Choi, I.H. Choi, Y.C. Shin, S.G. Ko, Induction of apoptotic cell death by ursolic acid through mitochondrial death pathway and extrinsic death receptor pathway in MDA-MB-231 cells, Arch. Pharm. Res. 34 (2011) 1363–1372.
[34] J. Li, X. Liang, X. Yang, Ursolic acid inhibits growth and induces apoptosis in gemcitabine-resistant human pancreatic cancer via the JNK and PI3K / Akt / NF- κ B pathways, Oncol. Rep. 28 (2012) 501–510.
[35] S. Saraswati, S.S. Agrawal, A.A. Alhaider, Chemico-biological interactions ursolic acid inhibits tumor angiogenesis and induces apoptosis through mitochondrial-dependent pathway in ehrlich ascites carcinoma tumor, Chem. Biol. Interact. 206 (2013) 153–165.
[36] Y. Li, X. Lu, H. Qi, X. Li, X. Xiao, J. Gao, Ursolic acid induces apoptosis through mitochondrial intrinsic pathway and suppression of ERK1/2 MAPK in He La cells, J. Pharmacol. Sci. 210 (2014) 202–210.
[37] H. Son, H.Y. Kwon, E.J. Sohn, J. Lee, H. Woo, M. Yun, S. Kim, Y. Kim, Activation of AMP-activated protein kinase and phosphorylation of glycogen synthase kinase3 b mediate ursolic acid induced apoptosis in HepG2 liver, Cancer Cells (2013).
[38] S. Shen, Y. Zhang, R. Zhang, X. Tu, X. Gong, Ursolic acid induces autophagy in U87MG cells via ROS-dependent endoplasmic reticulum stress, Chem. Biol. Interact. (2014).
[39] S. Leng, Y. Hao, D. Du, S. Xie, L. Hong, H. Gu, X. Zhu, J. Zhang, D. Fan, H.K. Kung, Ursolic acid promotes cancer cell death by inducing Atg5-dependent autophagy, Int. J. Cancer 133 (2013) 2781–2790.
[40] S.W. Shin, S.Y. Kim, J. Park, Biochimica et biophysica acta autophagy inhibition enhances ursolic acid-induced apoptosis in PC3 cells, BBA – Mol. Cell Res. 2012 (1823) 451–457.
[41] W. He, F. Shi, Z.-W. Zhou, B. Li, K. Zhang, X. Zhang, C. Ouyang, S.-F. Zhou, X. Zhu, A bioinformatic and mechanistic study elicits the antifibrotic effect of ursolic acid through the attenuation of oxidative stress with the involvement of ERK, PI3K/Akt, and p38 MAPK signaling pathways in human hepatic stellate cells and rat liver, Drug Des. Devel. Ther. 9 (2015) 3989–4104.
[42] D. Kashyap, H.S. Tuli, A.K. Sharma, Ursolic acid (UA): A metabolite with promising therapeutic potential, Life Sci. 146 (2016) 201–213.
[43] J. Iqbal, B.A. Abbasi, R. Ahmad, T. Mahmood, S. Kanwal, B. Ali, A.T. Khalil, S.A. Shah, M.M. Alam, H. Badshah, Ursolic acid a promising candidate in the therapeutics of breast cancer: current status and future implications, Biomed. Pharmacother. 108 (2018) 752–756.
[44] X. Zhang, X. Song, S. Yin, C. Zhao, L. Fan, H. Hu, p21 induction plays a dual role in anti-cancer activity of ursolic acid, Exp. Biol. Med. (Maywood) 241 (2016) 501–508.
[45] A. Dufner, M. Andjelkovic, B.M. Burgering, B.A. Hemmings, G. Thomas, Protein kinase B localization and activation differentially affect S6 kinase 1 activity and eukaryotic translation initiation factor 4E-binding protein 1 phosphorylation, Mol. Cell. Biol. 19 (1999) 4525–4534.
[46] M.A. Lohrum, M. Ashcroft, M.H. Kubbutat, K.H. Vousden, Identification of a cryptic nucleolar-localization signal in MDM2, Nat. Cell Biol. 2 (2000) 179–181.
[47] Q. Yang, L. Liao, X. Deng, R. Chen, N.S. Gray, J.R. Yates, J.D. Lee, BMK1 is involved in the regulation of p53 through disrupting the PML-MDM2 interaction, Oncogene 32 (2013) 3156–3164.
[48] E.F. Pettersen, T.D. Goddard, C.C. Huang, G.S. Couch, D.M. Greenblatt, E.C. Meng, T.E. Ferrin, UCSF Chimera - a visualization system for exploratory research and analysis, J. Comput. Chem. 25 (2004) 1605–1612.
[49] T.A. Halgren, Merck molecular force field. I. Basis, form, scope, parameterization, and performance of MMFF94, J. Comput. Chem. 17 (1996) 490–519.
[50] O. Trott, A.J. Olson, Autodock vina: improving the speed and accuracy of docking with a new scoring function efficient optimization, and multithreading, J. Comput. Chem. 31 (2010) 455–461.
[51] J.F. Blake, N.C. Kallan, D. Xiao, R. Xu, J.R. Bencsik, N.J. Skelton, K.L. Spencer, I.S. Mitchell, R.D. Woessner, S.L. Gloor, T. Risom, S.D. Gross, M. Martinson, T.H. Morales, G.P. Vigers, B.J. Brandhuber, Discovery of pyrrolopyrimidine inhibitors of Akt, Bioorg. Med. Chem. Lett. 20 (2010) 5607–5612.
[52] B. Anil, C. Riedinger, J.A. Endicott, M.E. Noble, The structure of an MDM2-nutlin-3a complex solved by the use of a validated MDM2 surface-entropy reduction mutant, Acta Crystallogr. 69 (2013) 1358–1366.
[53] J.C. Phillips, R. Braun, W. Wang, J. Gumbart, E. Tajkhorshid, E. Villa, C. Chipot, R.D. Skeel, L. Kalé, K. Schulten, Scalable molecular dynamics with NAMD, J. Comput. Chem. 26 (2005) 1781–1802.
[54] V. Zoete, M.A. Cuendet, A. Grosdidier, O. Michielin, SwissParam: a fast force field generation tool for small organic molecules, J. Comput. Chem. 32 (2011) 2359–2368.
[55] A.D. MacKerell, D. Bashford, M. Bellott, R.L. Dunbrack, J.D. Evanseck, M.J. Field, S. Fischer, J. Gao, H. Guo, S. Ha, D. Joseph-McCarthy, L. Kuchnir, K. Kuczera, F.T. Lau, C. Mattos, S. Michnick, T. Ngo, D.T. Nguyen, B. Prodhom, W.E. Reiher, B. Roux, M. Schlenkrich, J.C. Smith, R. Stote, J. Straub, M. Watanabe, J. Wiórkiewicz-Kuczera, D. Yin, M. Karplus, All-atom empirical potential for molecular modeling and dynamics studies of proteins, J. Phys. Chem. B 102 (1998) 3586–3616.
[56] W. Humphrey, A. Dalke, K. Schulten, VMD: visual molecular dynamics, J. Mol. Graph. 14 (33–8) (1996) 27–28.
[57] H. Attouch, R. Cominetti, A dynamical approach to convex minimization coupling approximation with the steepest descent method, J. Differ. Equ. 128 (1996) 519–540.
[58] T. Mosmann, Rapid colorimetric assay for cellular growth and survival: application to proliferation and cytotoxicity assays, J. Immunol. Methods 65 (1983) 55–63.
[59] S. Kasibhatla, D. Amarante-Mendes, G.P. Finucane, T. Brunner, E. Bossy-Wetzel, D.R. Green, Acridine orange/ethidium bromide (AO/EB) staining to detect apoptosis, Cold Spring Harb. Protoc. (2006).